THEORETICAL CHEMISTRY INSTITUTE

THE UNIVERSITY OF WISCONSIN

CALCULATED COLLISION INDUCED ABSORPTION SPECTRUM FOR He-Ar

by

D. A. McQuarrie

and

R. B. Bernstein

TIS-TCI-287

1 March 1968

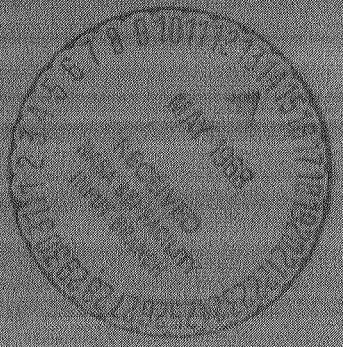

MADISON, WISCONSIN

CALCULATED COLLISION INDUCED ABSORPTION SPECTRUM FOR He-Ar*

by

D. A. McQuarrie

Theoretical Chemistry Institute, University of Wisconsin and

Science Center, North American Rockwell Corporation,

Thousand Oaks, California

and

R. B. Bernstein

Theoretical Chemistry Institute and Chemistry Department

University of Wisconsin, Madison, Wisconsin

ABSTRACT

Computations (exact within the classical framework) are presented of the translational absorption spectrum for a model system of dissimilar rare gas atoms chosen to simulate the He-Ar pair. The treatment makes use of the classical theory of Levine and Birnbaum. However, the procedure takes proper account of the non-linear collision trajectories (evaluated on the basis of a realistic interaction potential derived from beam scattering experiments) and the theoretical form of the dipole moment function (i.e., the *ab initio* computations of Matcha and Nesbet). The calculations reproduce the experimental (Bosomworth and Gush) line shape for He-Ar fairly well, provided the "dipole range parameter" is altered by some 7% from its *ab initio* value.

- - - - -

* Research supported by National Aeronautics and Space Administration Grant NsG-275-62.

I. Introduction

Translational absorption spectra or collision-induced absorption (CIA) curves were first observed in rare gas mixtures in the infrared by Kiss and Welsh[1] in 1959. They correctly attributed this absorption to the transient electric dipole moment formed during a close encounter between two dissimilar rare gas atoms. They observed only the high frequency wing of the absorption band ($\gtrsim 350$ cm^{-1}). The complete band was later seen by Bosomworth and Gush,[2] working in the far infrared. They were able to observe absorption for helium-argon and neon-argon mixtures, but for helium-neon the absorption was too weak to be observed. The CIA curves are broad bands starting at very low frequencies and extending over a range of several hundred wave numbers, with a broad maximum occurring in the region 100-200 cm^{-1}.

The first detailed theoretical discussion of collision induced (or "translational") absorption is that of Poll and van Kranendonk,[3] who have derived expressions for the integrated absorption coefficients in terms of a quadrature involving the intermolecular potential and the induced dipole moment. Their work did not yield a detailed line shape, however. This was first done by Tanimoto,[4] who employed a quantum mechanical formulation of absorption, the dipole moment matrix elements taken between scattering state wave functions. He used an exponentially decaying radial dependence both for the intermolecular potential and induced dipole moment. Since he did not solve the radial Schroedinger equation analytically,

he resorted to several approximations, of uncertain validity. In addition, the only data available for analysis were the less accurate high frequency wing results, so his evaluation of the parameters was such that the computed overall line shape was unreliable. In principle, however, he completely solved the line shape problem.

This work was followed by the independent work of Levine and Birnbaum[5] who calculated the line shape classically, employing classical radiation theory to determine the emission spectrum and converting this to absorption by means of Kirchoff's law. By using a simple modified gaussian-type radial function to describe the induced dipole moment function, and assuming straight-line trajectories, an analytic expression was obtained for the entire spectrum which could be well-fitted to the experimental data. Thus, they were the first to be able to reproduce the complete line shape. This work was followed by Futrelle,[6] who studied the dependence of the CIA (particularly, frequency moments of the absorption band) on the repulsive part of the interaction potential. He found that the temperature dependence of the absorption is a much more sensitive probe into the atomic potential than some of the more conventional techniques (e.g., the second virial coefficient or transport properties). He also emphasized the important qualitative difference in sensitivity between virial and transport data and CIA observations. In the former, the measurements contain substantial contributions from like atom interactions, and it is difficult to obtain by "subtraction" of suitable combinations

of data information on the unlike atom interaction (V_{ab}). Since it is the V_{ab} that contributes to the CIA, this method has the possibility of being a direct probe into unlike interactions. The only other experiments yielding this information are elastic scattering of atomic beams and thermal diffusion coefficients.

All of the above assumes that the dipole moment function is known. This function can in principle be obtained from a quantum mechanical calculation; within the Hartree-Fock approximation this has been done by Matcha and Nesbet.[7] They found that $\mu(r)$ can be well-fitted by an exponentially decaying radial function. This form has been used in all the theoretical investigations except that of Ref. 5. Even though the numerical values of the Hartree-Fock evaluated $\mu(r)$ are approximate, the functional form (exponential) is probably quite realistic. Thus, if the interatomic potential were known, the CIA data could yield the parameters of the expotential function for $\mu(r)$. Futrelle[8] has studied the dependence of various moments of the absorption data on both $\mu(r)$ and the potential and has shown how to separate the effect of these two unknown quantities. Most recently, Okada, Kajikawa, and Yamamoto[9] have calculated absorption curves for a hard-sphere potential and an exponentially decreasing dipole moment function. This was done by way of the dipole moment autocorrelation function approach.[10]

In view of the above, it seems desirable to carry out an exact computation of a line shape for a realistic dipole moment

function and interatomic potential, using the classical electrodynamic method of Levine and Birnbaum but employing exact classical trajectories. Many of the integrals that appear are similar to those studied by Bernstein and Kramer[11] in the application of the sudden approximation to the rotational excitation of molecules by atoms. The present paper thus reports line shape calculations for an exponential dipole moment function and a Lennard-Jones (12,6) interaction potential. The dependence of the line shape on the various parameters of the system is explored. The results can serve as an exact "model calculation" against which various approximate theories may be compared.

II. General Relations

The starting point of Levine and Birnbaum's[5] analysis is Kirchhoff's law, relating the absorption coefficient $A(\omega)$ to the power due to spontaneous emission per unit frequency interval per unit volume of sample $I(\omega)$:

$$A(\omega) = I(\omega)/c\, u(\omega) \qquad (1)$$

where c is the speed of light and $u(\omega)$ is the density of black body radiation. Levine and Birnbaum argue that the Rayleigh-Jeans law is the appropriate form of $u(\omega)$ to be used; despite the fact that $\hbar\omega/kT$ is not $\ll 1$ over much of the range of the

experimental data; thus:

$$u(\omega) \cong \omega^2 kT/\pi^2 c^3 \quad . \tag{2}$$

The quantity $I(\omega)$ can be written as an average over power from various classes of collisions,

$$I(\omega) = \iint N(b,E)\ \hat{I}(\omega, b, E)\, db\, dE \tag{3}$$

where $N(b,E)dbdE$ is the number of collisions per unit volume per unit time with impact parameter in the range $b, b + db$ and relative energy in the range $E, E + dE$; assumed known from kinetic theory. The emission intensity $\hat{I}(\omega,b,E)$ is obtained from Larmor's formula for the power emitted by an accelerating charge.[12] In terms of the induced dipole moment $\hat{I}(\omega,b,E)$ is given by

$$\hat{I}(\omega, b, E) = \frac{2\omega^4}{3c^3\pi} \left| \int_{-\infty}^{\infty} dt\, e^{i\omega t} \underset{\sim}{\mu}(b, E, t) \right|^2 \tag{4}$$

where $\underset{\sim}{\mu}(b,E,t)$ is the transient dipole moment of the colliding pair. It is assumed that the dipole moment is directed along the internuclear axis and a function only of the scalar magnitude of the distance, i.e. $\underset{\sim}{\mu}(\underset{\sim}{r}) = \frac{\underset{\sim}{r}}{r}\mu(r)$.

It is through r that μ depends upon t, b, and E, i.e., through the dynamics of the collision. It is here, of course, that the interaction potential exerts its influence.

A convenient coordinate system in which to decompose $\underset{\sim}{\mu}(r(t))$ is the cartesian system shown in Fig. 1. Noting the angle $\phi(t)$ in Fig. 1, one writes

$$\mu_x(t) = \mu(r(t)) \cos \phi(t) \tag{5}$$

$$\mu_y(t) = \mu(r(t)) \sin \phi(t) \, . \tag{6}$$

In terms of more conventional angles used in classical collision theory,

$$\phi(t) = \frac{\pi}{2} - \theta_o + \theta(t) = \theta(t) + \chi/2 \; ; \tag{7}$$

here θ_o is the angle between the apse line and the x' axis (incoming trajectory) and χ is the angle of deflection. The zero of time is taken to be that at which r assumes its minimum value, r_o. With this choice of the origin of time, $\mu_x(t)$ and $\mu_y(t)$ are odd and even functions of time, respectively, and so

$$\hat{I}(\omega, b, E) = \frac{8\omega^4}{3\pi c^3}\left\{\left|\int_0^\infty dt\, \mu_x(t) \sin \omega t\right|^2 + \left|\int_0^\infty dt\, \mu_y(t) \cos \omega t\right|^2\right\} \tag{8}$$

At this point the functional form of the dipole moment function must be introduced. Computations[7] showed that $\mu(r)$ can be fitted closely by a simple exponential function over the entire range of interatomic separations considered, viz. $2.0 < r < 5.5$ a.u.

$$\mu(r) = \mu_0 \exp(-r/\rho) \tag{9}$$

Matcha and Nesbet[7] report values of μ_0 and ρ for the rare gas pairs He-Ne, He-Ar, and Ne-Ar. Substituting Eq. (9) into Eq. (8), letting $\tau = \omega t$, one obtains

$$\hat{I}(\omega, b, E) = \frac{8\mu_0^2\omega^2}{3\pi c^3}\left(I_1^2 + I_2^2\right) \tag{10}$$

where

$$I_1 = \int_0^\infty d\tau \sin \tau\, f_1(\tau) \tag{11a}$$

$$I_2 = \int_0^\infty d\tau \cos \tau\, f_2(\tau) \tag{11b}$$

and

$$f_1(\tau) = e^{-r(\tau)/\rho} \cos\phi(\tau) \tag{12a}$$

$$f_2(\tau) = e^{-r(\tau)/\rho} \sin\phi(\tau) \tag{12b}$$

The time evolution of $f_1(\tau)$ and $f_2(\tau)$ is determined by the collision dynamics of the colliding pair. From classical collision theory one has

$$\theta(y) = \int_0^y dy / F(y) \tag{13}$$

and

$$t(y) = \left(\frac{m}{2E}\right)^{1/2} \int_{y_0}^{y} dy / y^2 F(y) \tag{14}$$

In Eqs. (13) and (14), m is the reduced mass of the colliding pair, $y \equiv b/r$, and

$$F(y) \equiv \left[1 - y^2 - V(y)/E\right]^{1/2} \tag{15}$$

where E is the collision energy and V(y) is the potential energy function; y_o is given by the inner root (corresponding to the outer turning point) of $F(y_o) = 0$.

The interatomic potential is not known with great precision even for rare gas atoms. Matcha and Nesbet have calculated V(r) for the rare gas pairs in the same Hartree-Fock basis used for $\mu(r)$; although it would perhaps be more consistent to use this V(r) in the present calculation, it is well known that such potentials (obtained in the Hartree-Fock approximation) are purely repulsive. However, direct atomic beam scattering measurements at thermal energies have indicated the need for attractive "tails", and so the standard "experimental" Lennard-Jones (12,6) potential may be more realistic and preferable in the present application. Thus it is assumed that

$$V(r) = 4\epsilon\left[\left(\frac{\sigma}{r}\right)^{12} - \left(\frac{\sigma}{r}\right)^{6}\right] \tag{16}$$

$$= 4\epsilon\left[\left(\frac{\sigma y}{b}\right)^{12} - \left(\frac{\sigma y}{b}\right)^{6}\right]$$

where σ and ϵ have their usual meanings. To reduce the lengths and energies that appear in the calculation, quantities are defined such as $b^* \equiv b/\sigma$, $\rho^* \equiv \rho/\sigma$, $E^* \equiv E/\epsilon$, $V^* \equiv V/\epsilon$. In terms of these reduced quantities, Eq. 14 becomes

$$\tau(y) = \omega\sigma\cdot\left(\frac{m}{2\epsilon}\right)^{1/2}\cdot J(y, E^*, b^*) \tag{17}$$

where

$$J(y, E^*, b^*) \equiv \frac{b^*}{E^{*1/2}} \int_{y_0}^{y} dy / y^2 F(y, b^*, E^*) \quad . \quad (18)$$

Eqs. 13 and 18 now express $\theta(y)$ and $\tau(y)$ as functions of the reduced impact parameter b^* and the reduced energy E^*. These can be inverted to give $y(\tau)$ or $r(\tau)$ and $\theta(\tau)$ or $\phi(\tau)$, which are used to evaluate $f_1(\tau)$ and $f_2(\tau)$, then I_1 and I_2, and finally $\hat{I}(\omega, b^*, E^*)$. A quantity $\alpha(\omega, b^*, E^*)$ is defined by

$$\alpha(\omega, b^*, E^*) \equiv \frac{3\pi c^3}{8\mu_0^2 \omega^2} \cdot \hat{I}(\omega, b^*, E^*) \quad (19)$$

The total power emitted per unit frequency interval per unit volume is

$$I(\omega) = \int\int N(b^*, E^*) \hat{I}(\omega, b^*, E^*) db^* dE^* \quad (20)$$

where

$$N(b^*, E^*) = 4\pi n_A n_B \sigma^2 \cdot \left(\frac{2\epsilon}{\pi m}\right)^{1/2} \cdot \frac{E^{*2} b^*}{T^{*3/2}} \cdot e^{-E^*/T^*} \quad (21)$$

In Eq. 21, n_A and n_B are the numbers of molecules per unit volume of the two colliding species and $T^* \equiv kT/\epsilon$. Finally then, by Eqs. 1, 2, 19, 20, and 21:

$$A(\omega) = \frac{64}{3}\frac{\pi^{3/2}}{cT^{*5/2}}\cdot\frac{\mu_0^2\sigma^2}{(2m\epsilon)^{1/2}}\iint \alpha(\omega, b^*, E^*)E^* e^{-E^*/T^*} b^* db^* dE^*. \tag{22}$$

Assuming that the rare gas mixtures are ideal at 0°C and 1 atms., then

$$n_{A,B} = 2.687 \times 10^{19} d_{A,B} \text{ (amagat)} \tag{23}$$

and the quantity presented experimentally by Bosomworth and Gush[2] is

$$\frac{A(\omega)}{d_A d_B} = \frac{2.861\times 10^{30}\mu_0^2\sigma^2}{(2\epsilon m)^{1/2}T^{*5/2}}\iint \alpha(\omega, b^*, E^*)E^* e^{-E^*/T^*} b^* db^* dE^* \tag{24}$$

where d_A and d_B are densities expressed in amagats. The calculation of $A(\omega)$ and particularly the calculation of $\alpha(\omega, b^*, E^*)$ and its integral over b^* and E^* will be discussed in detail in Sec. III. It is also of some interest to consider a relationship due to Poll and van Kranendonk,[3] viz.

$$\beta_2 \equiv \frac{1}{2\pi}\int_0^\infty \alpha(\omega)\, d\omega$$

$$= \frac{4\pi^2 n_A n_B}{3mc}\int_0^\infty \left[\left(\frac{d\mu}{dr}\right)^2 + \frac{2\mu^2}{r^2}\right] g(r)\, r^2 dr. \tag{25}$$

Here $g(r)$ is the radial distribution function, which for the present case is simply $\exp\left[-\beta u(r)\right]$. Poll and van Kranendonk[3] and Futrelle[8] have derived and used expressions for other moments of the spectrum.

III. Summary of Computational Procedures

The input parameters for the program are E^*, ρ^*, W, defined by $\omega\sigma(m/2\epsilon)^{\frac{1}{2}}$, and tables of predetermined values $y_0(b^*,E^*)$ and $\chi(b^*,E^*)$. Tables of $F(y)$, $\theta(y)$, and $J(y)$ are constructed, the latter two being evaluated by trapezoidal rule. For a "typical" case ($W = 32.4$ and $\rho^* = 0.125$), the interval size used in the integration was 0.001 (same for all values of E^*). The construction of these three tables is done only once (for the first value of W) since they are independent of W, and stored for subsequent use. Using Eq. 17,

$$\tau(y) = W J(y) . \qquad (26)$$

Incrementing τ by $\Delta\tau$ and interpolating for the corresponding values of J and y (and hence $\theta(y)$) yields the $y(\tau)$ and $\theta(\tau)$ to be used in the evaluation of I_1 and I_2 :

$$I_1 \equiv \int_0^\infty d\tau\, e^{-b^*/\beta^* y(\tau)} \cos\left[\theta(\tau) + \tau/2\right] \sin\tau \qquad (27a)$$

$$I_2 \equiv \int_0^\infty d\tau\, e^{-b^*/\beta^* y(\tau)} \sin\left[\theta(\tau) + \tau/2\right] \cos\tau \qquad (27b)$$

The interpolation referred to above is the Aitken method, typically using four points. The integrals in Eq. 27 are evaluated by trapezoidal rule, the upper limit being determined such that the change in the value of R ,

$$R \equiv b^* \times \left(I_1^2 + I_2^2\right) \qquad (28)$$

for the last two consecutive values of the upper limit is less than or equal to 2% of the value of R. (see Fig. 5). The program next determines the limit b^*_{max} of the integration of $R(b^*, E^*)$ over b^*. This integral is

$$D(E^*) \equiv \int_0^{b^*_{max}} R(b^*, E^*)\, db^* \qquad (29)$$

The maximum value of R(i.e., R_{max}) is searched out and the maximum allowable error is set to be 2% of R_{max}. The upper limit of b^* is sedected such that $R(b^*_{max}) \leq 1\%$ of R_{max}. The mesh size of τ in Eq. 27 is divided by 5 and the integrals

are recomputed at the value of b^* giving R_{max}. This is done up to three times until R_{max} changes by less than 2%. If the original mesh size is satisfactory the values of A already calculated are used in Eq. 29, otherwise the calculation is redone with a finer mesh. This recomputation requires obtaining again the necessary F(y), $\theta(y)$, and J(y) values for each W,b^*, and E^*, but this was seldom necessary. After a reliable R is obtained the program proceeds to the evaluation of $D(E^*)$. This is done by trapezoidal rule with a typical mesh size of 0.1. The last step is the integration of $D(E^*)$ over E^* to give the absorption (to within a multiplicative constant):

$$I \equiv \int_0^\infty dE^* \; D(E^*)\, E^* e^{-E^*/T^*} \tag{30}$$

It is convenient to transform the variable of integration from E^* to $z = \ln E^*$, to give

$$I = \int_0^\infty \mathcal{D}(z)\, dz$$

where

$$\mathcal{D}(z) \equiv D \exp\left[-\frac{e^z}{T^*} + 2z \right] \tag{31}$$

$\mathcal{D}(z)$ is calculated at all the values of E^* (viz., 1,2,3,5,10,20, 30,50 and 100); intermediate values are computed from an interpolation polynomial, which is then integrated to give I, the line shape

except for the multiplicative constant.

Figures 2-8 illustrate typical behavior of the various intermediate quantities defined above, starting with the integrands of I_1 and I_2 of Eq. 27 vs. τ and ending with I in Eq. 30. Figs. 2a and 2b show the integrands of I_1 and I_2 vs. τ, i.e. the $f_1(\tau) \sin\tau$ and $f_2(\tau) \cos\tau$ of Eq. 12 vs. τ for the parameters $b^* = 0.7$, $E^* = 10.0$, and $\rho^* = 0.125$. Fig. 2a is for $W = 16.2$ and 2b for $W = 32.4$. Next in the progression of the program is the quantity $A = I_1^2 + I_2^2$ vs. W which is shown in Fig. 3 for the parameters $b^* = 0.7$ and $E^* = 10.0$. The three curves for $\rho^* = 0.110$, 0.117, and 0.125 show increasing maxima. Figs. 3a and 3b show A vs. b^* for $E^* = 10.0$, $\rho^* = 0.125$ and $W = 16.2$ and 32.4, respectively. Next shown is $R \equiv b^*A$ vs. b^* in Figs. 5a and 5b, again for $E^* = 10.0$, $\rho^* = 0.125$ and $W = 16.2$ and 32.4. The integral of R over b^*, $D(E^*)$, vs. E^* is shown in Figs 6a and 6b for $\rho^* = 0.125$, and $W = 16.2$ and 32.4, respectively.

Until now the temperature has not entered the calculation. It first appears in the energy integration (through the distribution of relative velocities), and Figs 7a and 7b show the integrand $\mathcal{D}(z)$ plotted for $\rho^* = 0.125$, $T^* = 11.6$ (295°K), and $W = 16.2$ and 32.4. Lastly, Fig. 8 shows the result of the energy integration, i.e. I vs. W for $\rho^* = 0.125$ and $T^* = 11.6$ (295°K). This series of figures displays the progress of the computation as one proceeds to the complete line shape.

IV. Results

In this section the results of the calculations (Eq. 24) are presented, particularly their dependence on several of the input parameters. These are ρ, the range parameter of the dipole moment overlap function; μ_0, the strength of the dipole moment function; and σ_{LJ} and ϵ, the L.-J.(12,6) potential parameters. For the dipole moment function $\mu(r) = \mu_0 \exp(-r/\rho)$ for He-Ar, the constants were taken[7] to be μ_0 = 33.7 debyes and $\rho = 0.359 \times 10^{-8}$ cm. The potential parameters were taken from the molecular beam measurements of Düren et al[13]: $\sigma_{LJ} = 3.07 \times 10^{-8}$ cm., $\epsilon = 3.50 \times 10^{-15}$ ergs. For this quartet of parameters, $\rho^* \equiv \rho/\sigma_{LJ} = 0.117$ and the reduced temperature at which the data where obtained (295°K) is $T^* = 11.6$. Fig. 9 shows curves of A vs. σ (cm^{-1}) for the "range ratio" $\rho^* = 0.110$, 0.117, and 0.125. Comparison of the lowest curve with the experimental data of Fig. 11 shows that the $A(\sigma)$ values calculated with $\rho^* = 0.110$ are too small by nearly an order of magnitude. However, $A(\sigma)$ is extremely sensitive to ρ^*, as seen in Fig. 9. The highest curve, for $\rho^* = 0.1275$, was not actually computed, but obtained by a short extrapolation of $A(\sigma)$ vs. ρ^* for each frequency, in an attempt to obtain the best fit to the experimental data. (In view of the uncertainty in extrapolation, the $\rho^* = 0.1275$ curve must, of course, be considered only approximate). It can be seen from Figs. 11 that the calculated (extrapolated) results peak slightly to lower frequencies than the experimental data. Since the extrapolations were of a short range,

i.e. from 0.110-0.125 to 0.1275, they should be quite reliable. This is even more substantiated in Figs. 10 and 12, where the quantity $\tilde{A}(\sigma) \equiv A(\sigma)/\sigma$ is considered. Fig. 10 shows this function for the three values of ρ^* for which computations were performed and the one extrapolated curve. In this case the value $\rho^* = 0.1257$ (a much smaller extrapolation) seemed to give the best fit to the data; the comparison is shown in Fig. 12. In neither Fig. 10 nor 12 was any parameter other than ρ^* changed. It would, of course, be possible to adjust the potential somewhat to achieve a better fit, but the main purpose of the present study was not to "parametrize to a best fit" but to present a series of exactly calculated results for a given set of dipole and potential functions against which approximate theories of CIA may be tested. Figs. 13 and 14 show the behavior of $A(\sigma)$ and $\tilde{A}(\sigma)$ for $T = 200^{\circ}K$, $295^{\circ}K$, and $400^{\circ}K$ for the optimum value of ρ^*. (As before, these curves were obtained by a slight extrapolation of the three curves computed for $\rho^* = 0.110, 0.117, 0.125$.) In Fig. 15 are presented a set of computed curves of $A(\sigma)$ for a series of temperatures, for $\rho^* = 0.125$. (These curves did not involve extrapolation.)

It should be emphasized that even though σ_{LJ} has been maintained fixed and ρ^* varied (and hence ρ itself), one could equally have fixed ρ and varied σ_{LJ}. However, since the factor in front in Eq. 24 contains only σ^2, the overwhelming effect comes from the ρ^* dependence of the integral. It seems that ρ

can be found quite independently of the potential by taking the ratio of the first two moments of the line shape,[14] viz. $\epsilon'(0)-1$ and Eq. (25), and so perhaps ρ can be considered better known than σ_{ij}. In view of the uncertainty of the functional form of both $\mu(r)$ and $u(r)$ however, this point is probably not worth belaboring.

V. Summary and Discussion

A number of curves of collision induced absorption line shapes have been computed in the spirit of the classical formulation of Levine and Birnbaum.[5] These have been calculated for a dipole moment overlap function suggested by the Hartree-Fock calculations of Matcha and Nesbet[7] and a Lennard-Jones (12,6) interatomic potential obtained from the scattering measurements of Düren et al.[13] The results are presented in figures showing not only the final absorption curves, but also a number of intermediate quantities which might be of interest in connection with any approximate theories. The results are found to be very sensitive to ρ^*, the ratio of the "ranges" of the dipole moment function and the interatomic potential. From Figs. 13, 14 and 15 it is seen that the results are only moderately sensitive to the value of the temperature, or to ϵ. It is also obvious (even without calculations) that the dependence on μ_0 is simple quadratic. The drastic dependence on ρ^*, shown in Figs. 9 and 11, indicates that a small change in ρ^*, from 0.110 to 0.125, i.e., $\approx 10\,\%$, gives rise to a change

in the absorption by nearly a factor of ten. Such a sensitivity is quite important and has heretofore not been noted. This implies that the experimental CIA results constitute an extremely sensitive method of deducing ρ^* ; on the other hand, however, it suggests that present ab initio calculations of ρ are not quite accurate enough to be practical input for collision induced absorption computations. Regarding the accuracy of the rare gas dipole moment calculations, Matcha[15] has stated that the main source of probable error in ρ is the lack of correlation terms in the electronic wave function. Adding such terms should increase the repulsion between electrons on separate atoms and thus heighten the distortion effect, tending to increase the induced dipole moment. All factors considered, an error of ca. $\pm$ 5% is not at all surprising.[15] All of this uncertainty does not even take into account the possible long range contribution to $\mu(r)$. The exponential form results from the short-range, non-correlation, calculation, but it is well-known that there should exist a long-range part similar to the long-range R^{-6} contribution to the potential (obtained from second order perturbation theory.[16] Buckingham[17] has shown that the first non-vanishing term in this long-range part goes as R^{-7} , but this has not been further considered.

The severe sensitivity to ρ is also seen in the integrated absorption, Eq. 25. Changing ρ^* in this quantity from 0.117 to 0.125 changes β_2 by a factor of ca. 2 . The value of $\rho^* = 0.125$ was chosen such that β_2 agreed with the measured integrated absorption.

The fact that the maximum in the line shape curve for this ρ^* was lower than for the experimental data seems to indicate that the calculated high frequency "tail" would be higher than experimental. Unfortunately, computations were not carried out at frequencies greater than ca. 240 cm^{-1} due to slow convergence of some of the integrals; however, the results are expected to be high, since a 50% discrepancy in β_2 must be accounted for. A similar behavior was found by Okada, Kajikawa, and Yamamoto[19] in their recent calculations based on a rigid sphere model.

In conclusion, the present paper has presented classical computations of the translational absorption spectrum for a model system (approximating He-Ar) taking account of the non-linear collision trajectories (based on experimental scattering studies) and the theoretical form of the (exponentially decaying) dipole moment function. With a change of only 7% in the value of the range of the dipole function from the ab initio value of Ref. 7 the experimental line shape was fairly well reproduced, confirming the essential correctness of the overall procedure.

Acknowledgment

The authors wish to express their appreciation to Mrs. C. Constable for her valuable assistance with the programming of the computations.

References

1. Z. J. Kiss and H. L. Welsh, Phys. Rev. Letters 2, 166 (1959).
2. D. R. Bosomworth and H. P. Gush, Can. J. Phys. 43, 751 (1965).
3. J. D. Poll and J. van Kranendonk, Can. J. Phys. 39, 189 (1961).
4. O. Tanimoto, Progr. Theoret. Phys. 33, 585 (1966).
5. H. B. Levine and G. Birnbaum, Phys. Rev. 154, 86 (1967).
6. R. P. Futrelle, Phys. Rev. Letters 19, 479 (1967).
7. R. L. Matcha and R. K. Nesbet, Phys. Rev. 160, 72 (1967).
8. R. P. Futrelle, to be published.
9. Okada, Kajikawa and Yamamoto, preprint.
10. R. G. Gordon, J. Chem. Phys. 44, 3083 (1966).
11. R. B. Bernstein and K. H. Kramer, J. Chem. Phys. 44, 4473 (1966).
12. J. D. Jackson, Classical Electrodynamics (John Wiley and Sons, Inc., New York, 1962), Chap. 14.
13. R. Düren, R. Feltgen, W. Gaide, R. Helbing and H. Pauly, Phys. Letts. 18, 282 (1965).
14. R. P. Futrelle and H. B. Levine, private communication, Feb. 1968.
15. R. L. Matcha, private communication, Oct. 1967.
16. J. O. Hirschfelder, W. B. Brown, and S. T. Epstein, in Advances in Quantum Chemistry (Academic Press, Inc., New York, 1964), Vol. I, p. 289.
17. A. D. Buckingham, Colloque sur les proprietés optiques et acoustiques des Fluides comprimes et les actions intermoléculaires, Bellevue, 1957.

Figure Legends

Fig. 1 Typical trajectory and coordinate system in which computations were performed.

Fig. 2a I_1 and I_2 vs. τ for $b^* = 0.7$, $E^* = 10.0$, $\rho^* = 0.125$, and $W = 16.2$.

Fig. 2b I_1 and I_2 vs. τ for $b^* = 0.7$, $E^* = 10.0$, $\rho^* = 0.125$, and $W = 32.4$.

Fig. 3 $A(b^*, E^*, \rho^*, W)$ vs. W for $b^* = 0.7$, $E^* = 10.0$, and $\rho^* = 0.110$, 0.117, and 0.125.

Fig. 4a $A(b^*, E^*, \rho^*, W)$ vs. b^* for $E^* = 10.0$, $\rho^* = 0.125$, and $W = 16.2$.

Fig. 4b $A(b^*, E^*, \rho^*, W)$ vs. b^* for $E^* = 10.0$, $\rho^* = 0.125$, and $W = 32.4$.

Fig. 5a R vs. b^* for $E^* = 10.0$, $\rho^* = 0.125$, and $W = 16.2$.

Fig. 5b R vs. b^* for $E^* = 10.0$, $\rho^* = 0.125$, and $W = 32.4$.

Fig. 6a $D(E^*, \rho^*, W)$ vs. E^* for $W = 16.2$.

Fig. 6b $D(E^*, \rho^*, W)$ vs. E^* for $W = 32.4$.

Fig. 7a $\mathcal{Q}(E^*, \rho^*, W)$ vs. E^* for $W = 16.2$.

Fig. 7b $\mathcal{Q}(E^*, \rho^*, W)$ vs. E^* for $W = 32.4$.

Fig. 8 I vs W at 295°K.

Fig. 9 $A(\sigma)$ vs σ for values of $\rho^* = 0.110$, 0.117, 0.125, 0.1275. The maximum of $A(\sigma)$ increases with increasing ρ^*.

Fig. 10 $\tilde{A}(\sigma) \equiv A(\sigma)/\sigma$ vs. σ for values of $\rho^* = 0.110$, 0.117, 0.125, 0.1275. The maximum of $\tilde{A}(\sigma)$ increases with increasing ρ^*.

Figure Legends (cont'd)

Fig. 11 Comparison of calculated vs. experimental $A(\sigma)$ for $\rho^* = 0.1275$ (extrapolated) and $T = 295^{\circ}K$.

Fig. 12 Comparison of calculated vs. experimental $\tilde{A}(\sigma)$ for $\rho^* = 0.1257$ (extrapolated) and $T = 295^{\circ}K$.

Fig. 13 $A(\sigma)$ vs. σ for $\rho^* = 0.1275$ (best value) for $T = 200^{\circ}K$, $295^{\circ}K$, and $400^{\circ}K$. The maxima increase and move toward higher frequencies with increasing temperature.

Fig. 14 $\tilde{A}(\sigma)$ vs. σ for $\rho^* = 0.1257$ (best value) for $T = 200^{\circ}K$, $295^{\circ}K$, and $400^{\circ}K$. The maxima decrease with increasing temperature.

Fig. 15 $A(\sigma)$ vs. σ for various temperatures and $\rho^* = 0.125$. These curves are computed (i.e., not obtained by extrapolation).

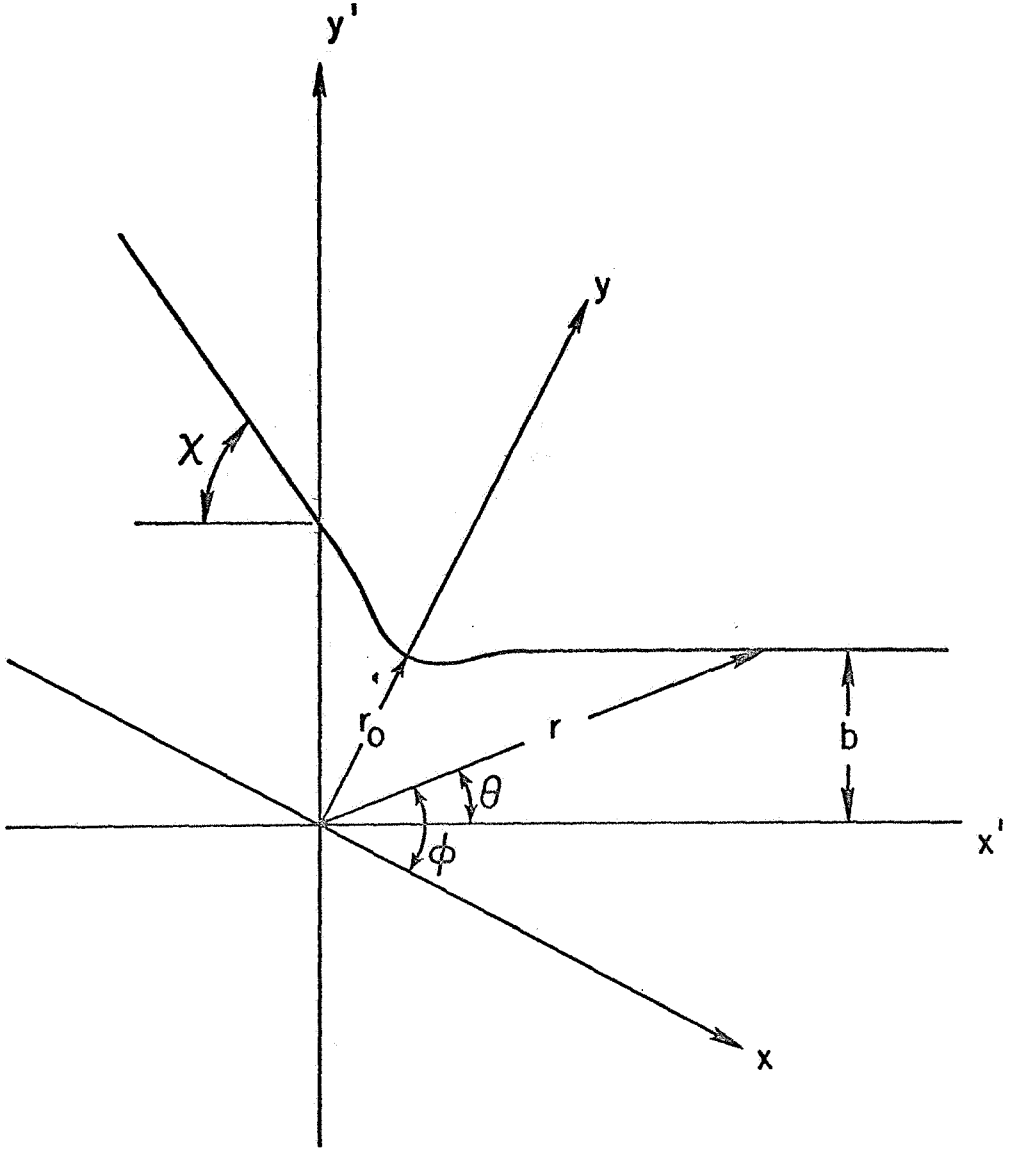

Figure 1

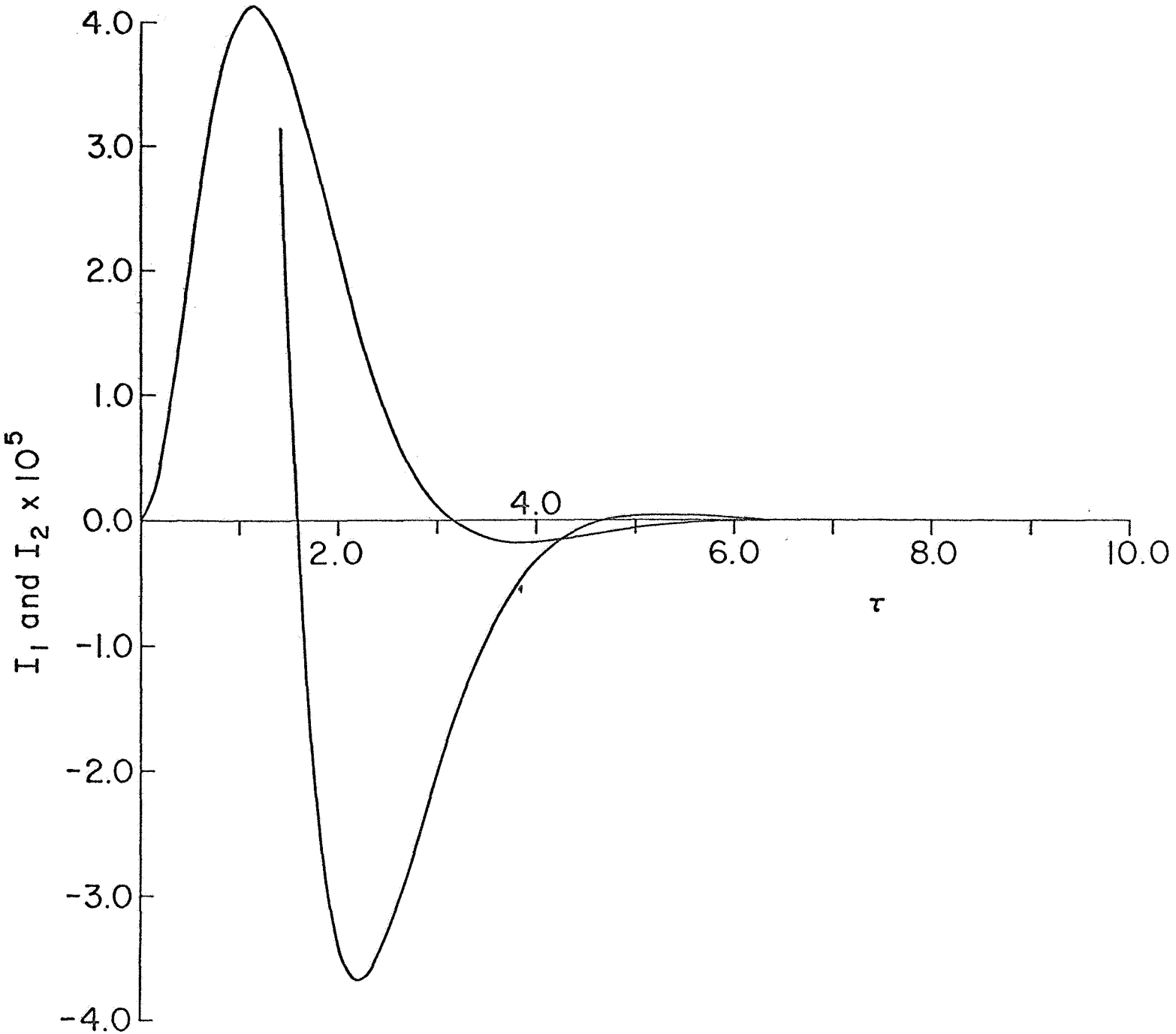

Figure 2a

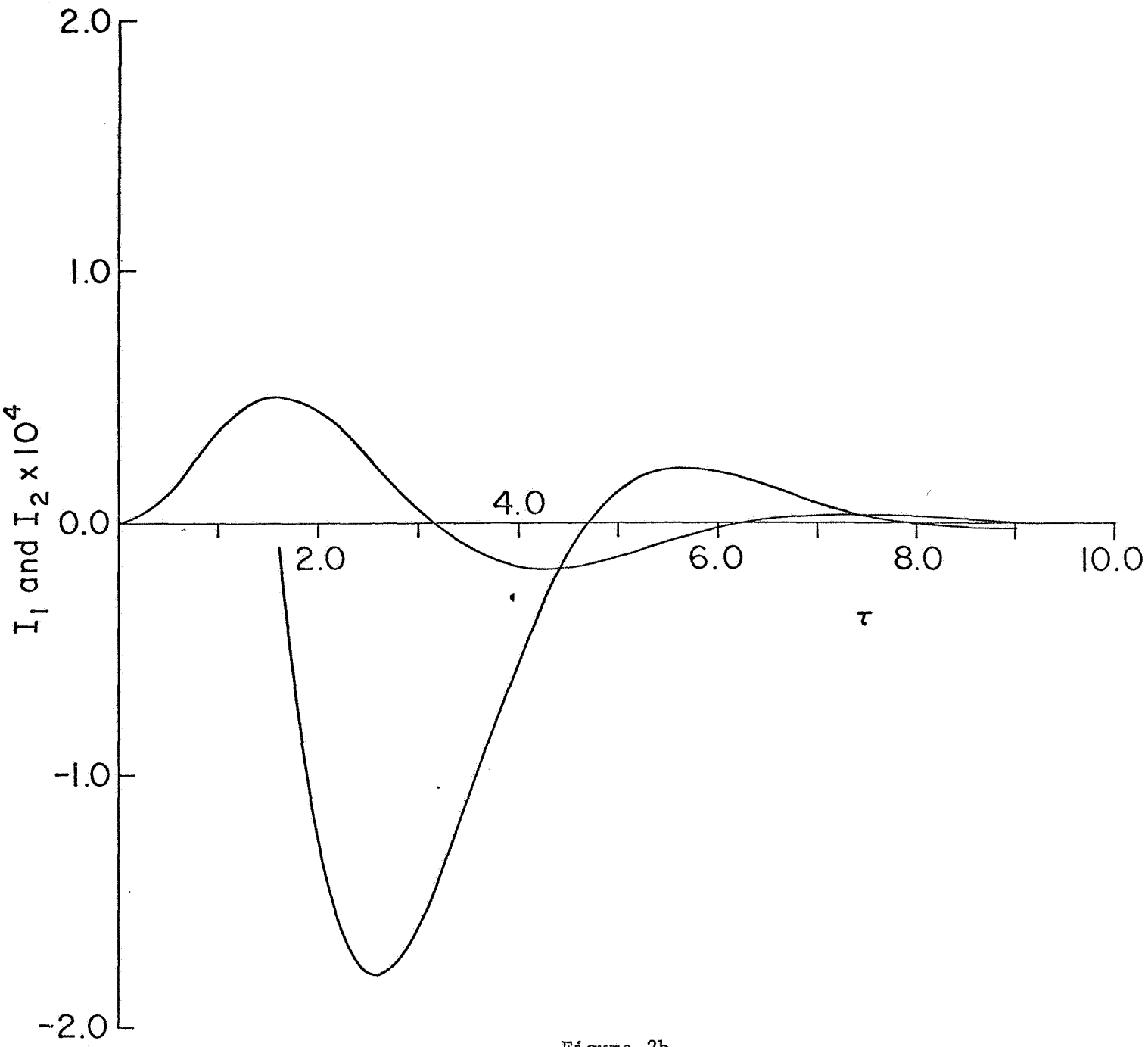

Figure 2b

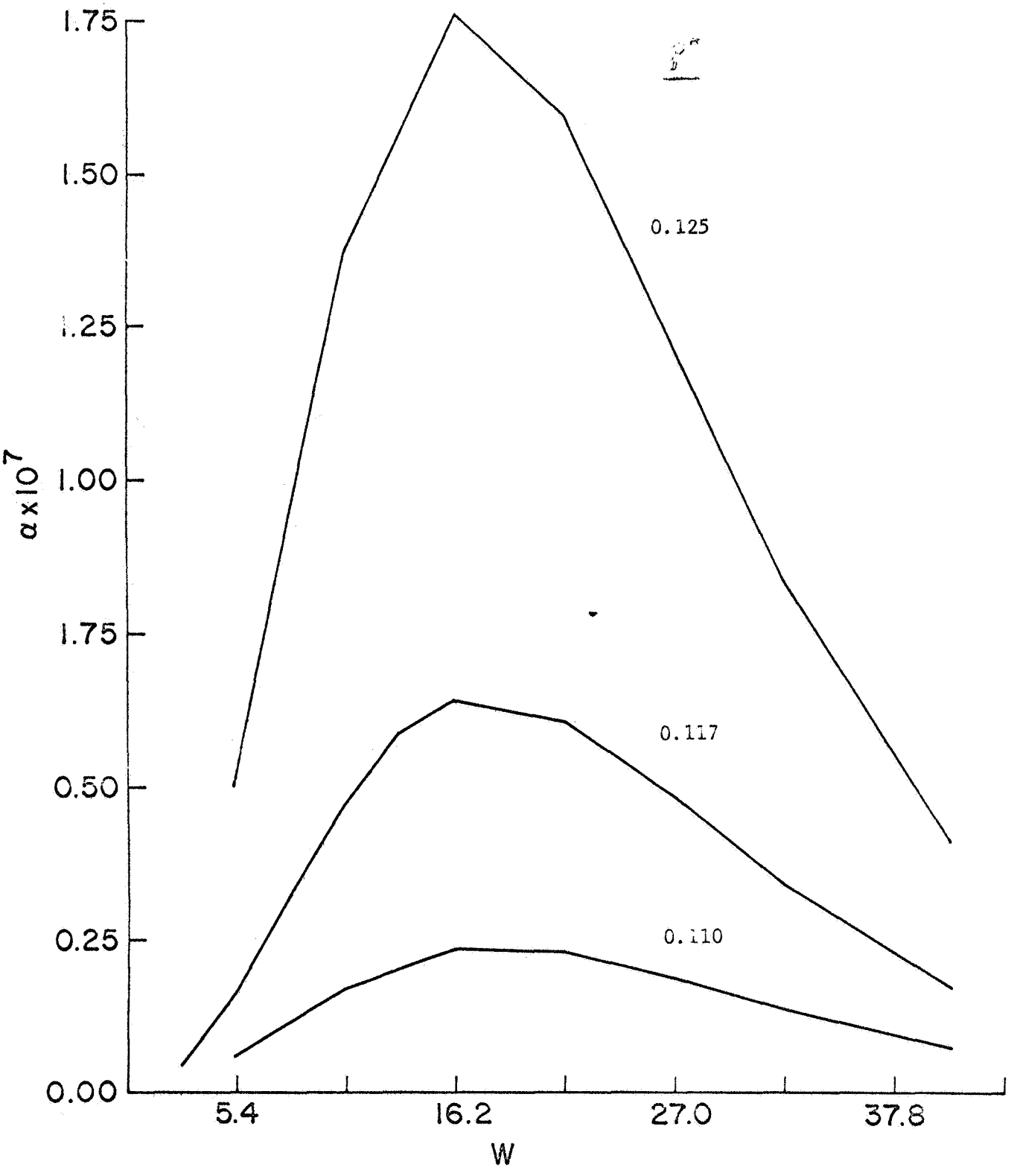
1.75
1.50
1.25
1.00
1.75
0.50
0.25
0.00
α x 10^7
0.125
0.117
0.110
5.4
16.2
27.0
37.8
W

Figure 3

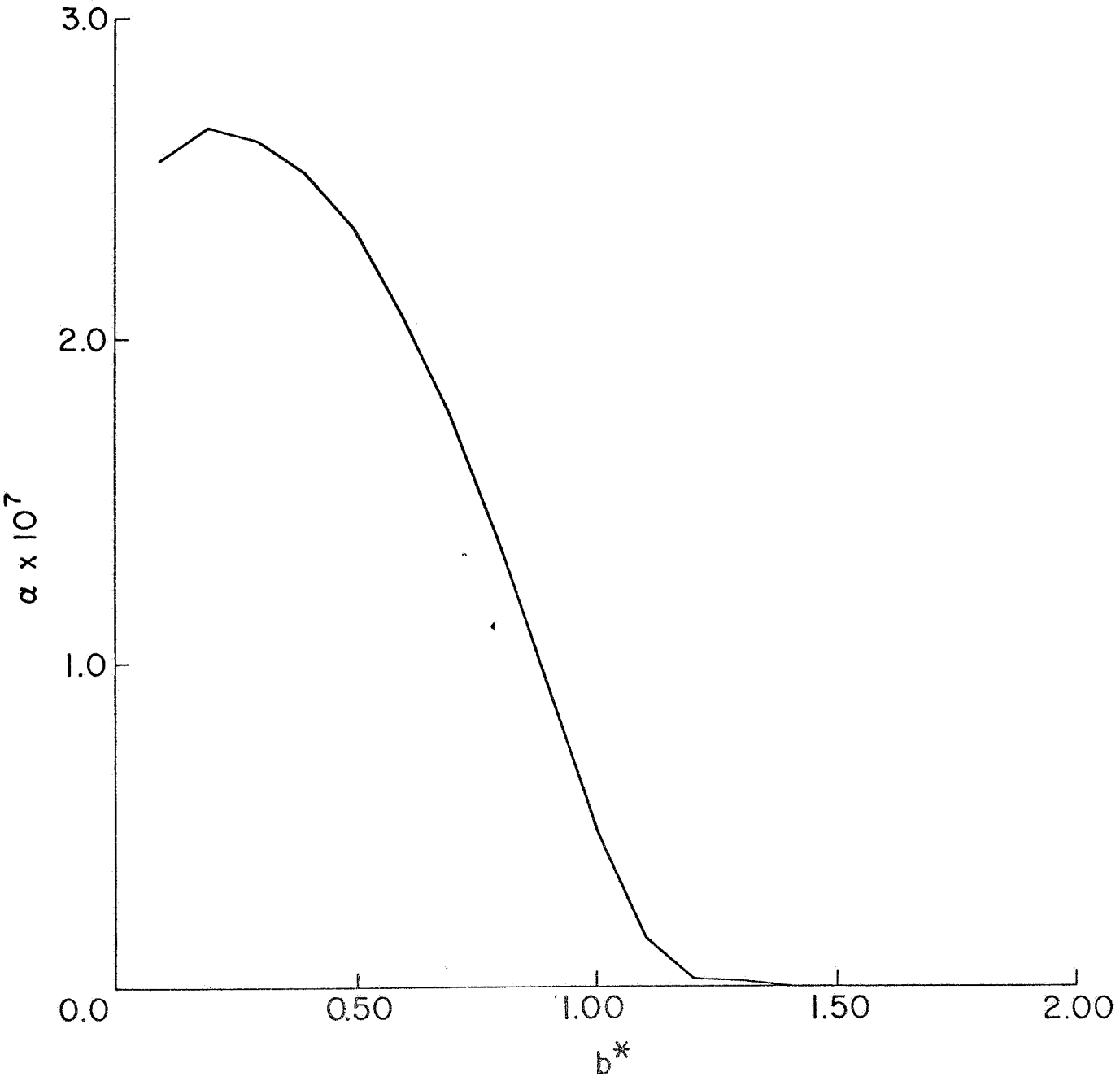

Figure 4a

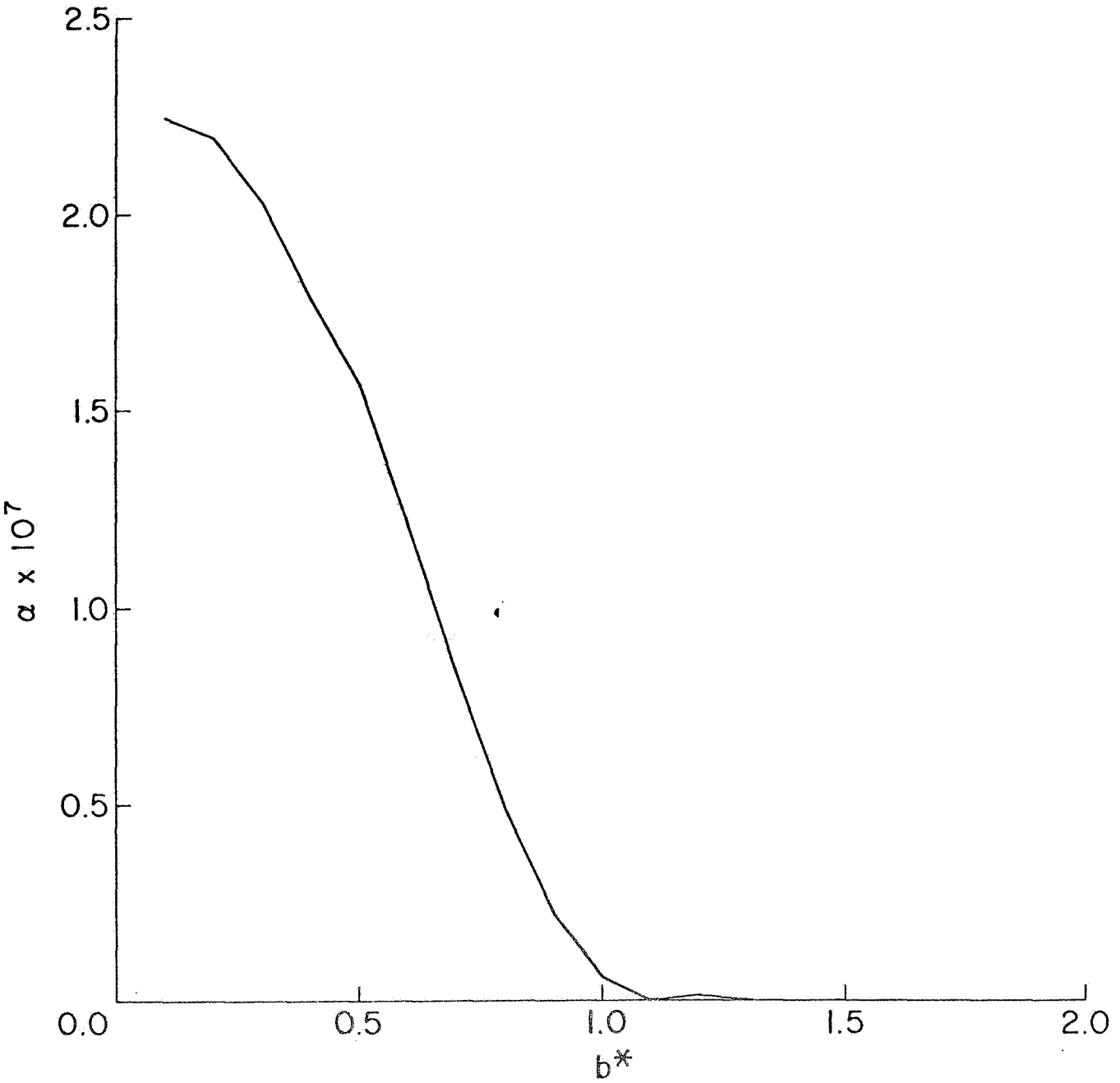

Figure 4b

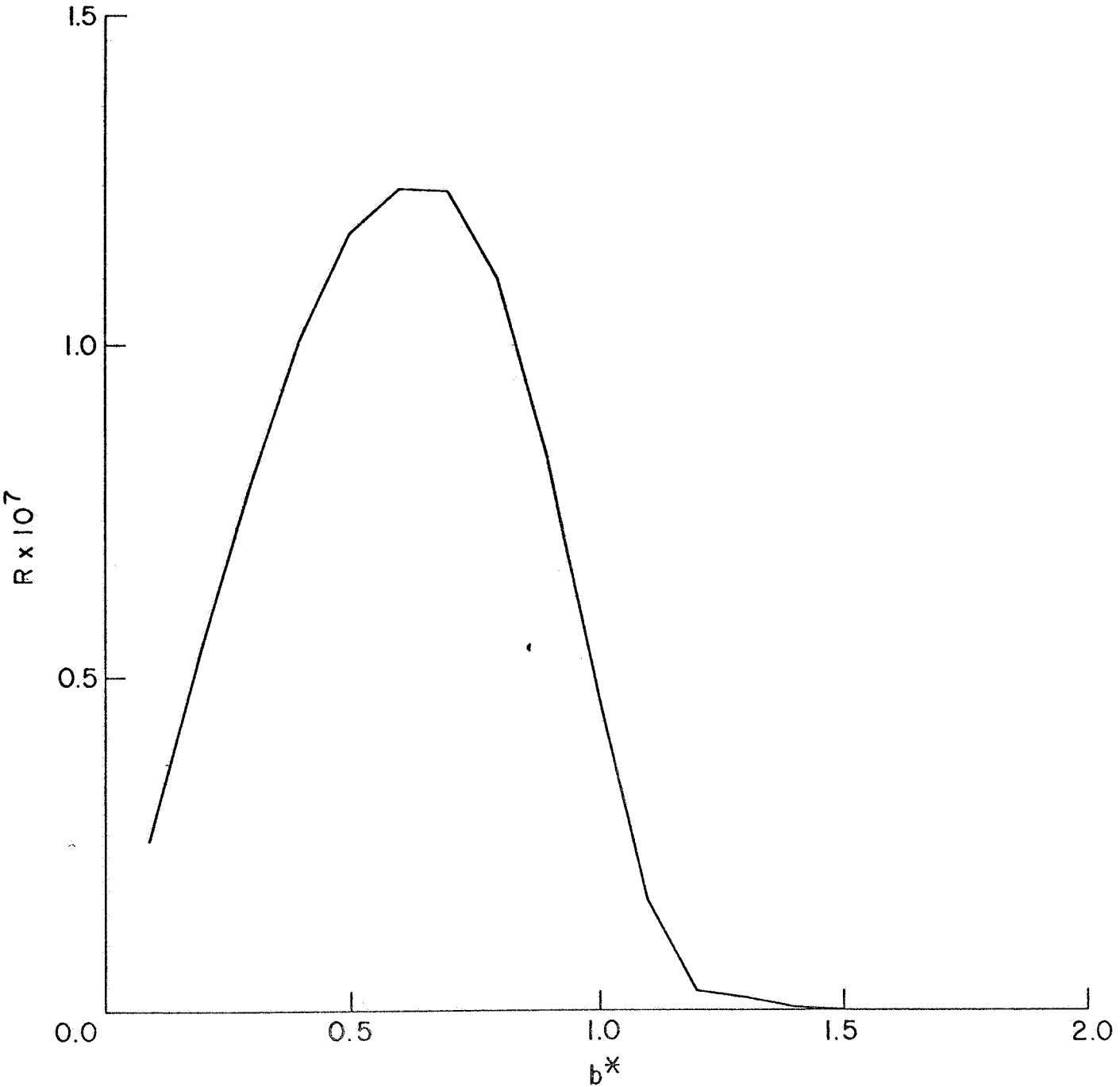

Figure 5a

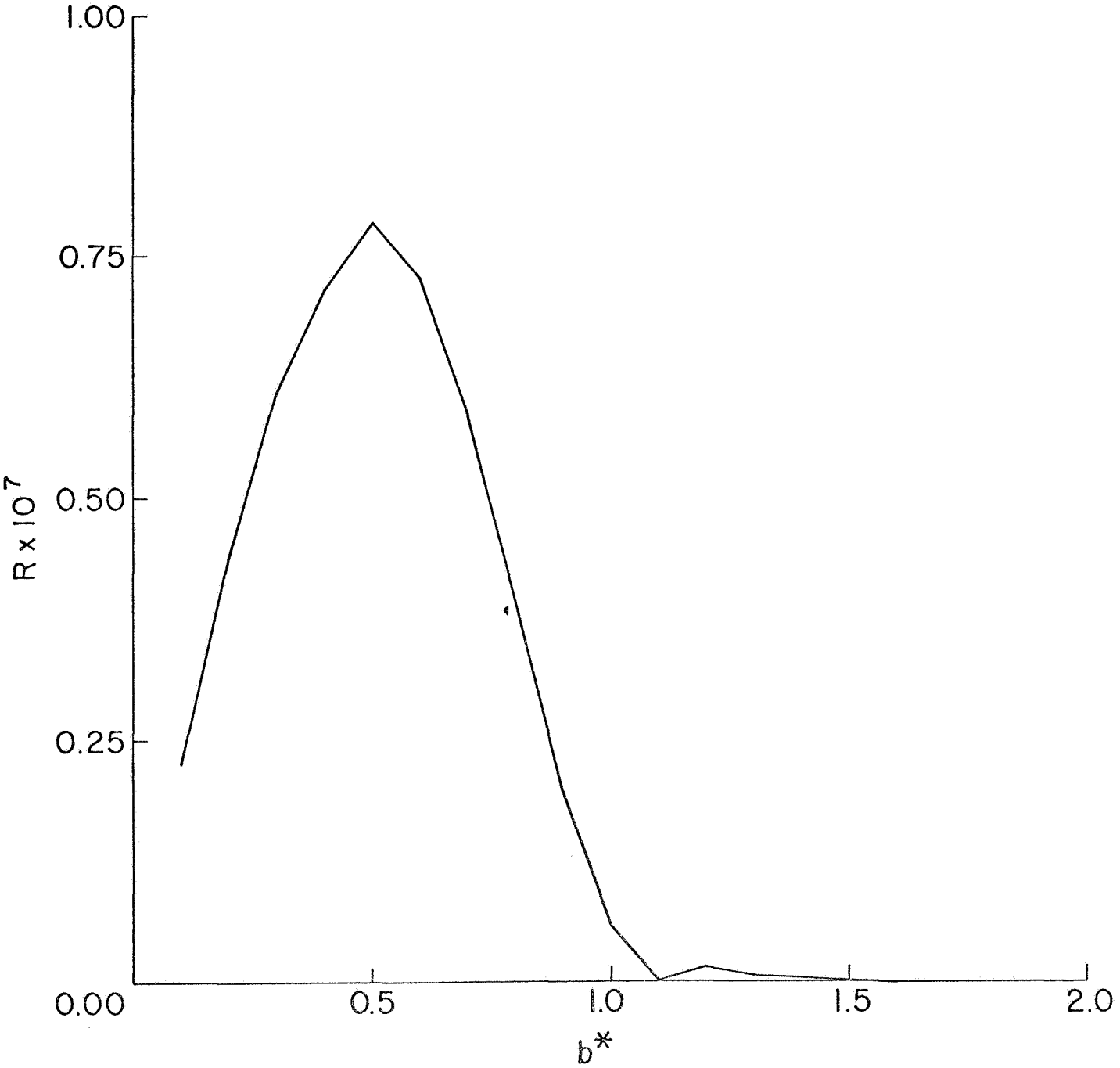

Figure 5b

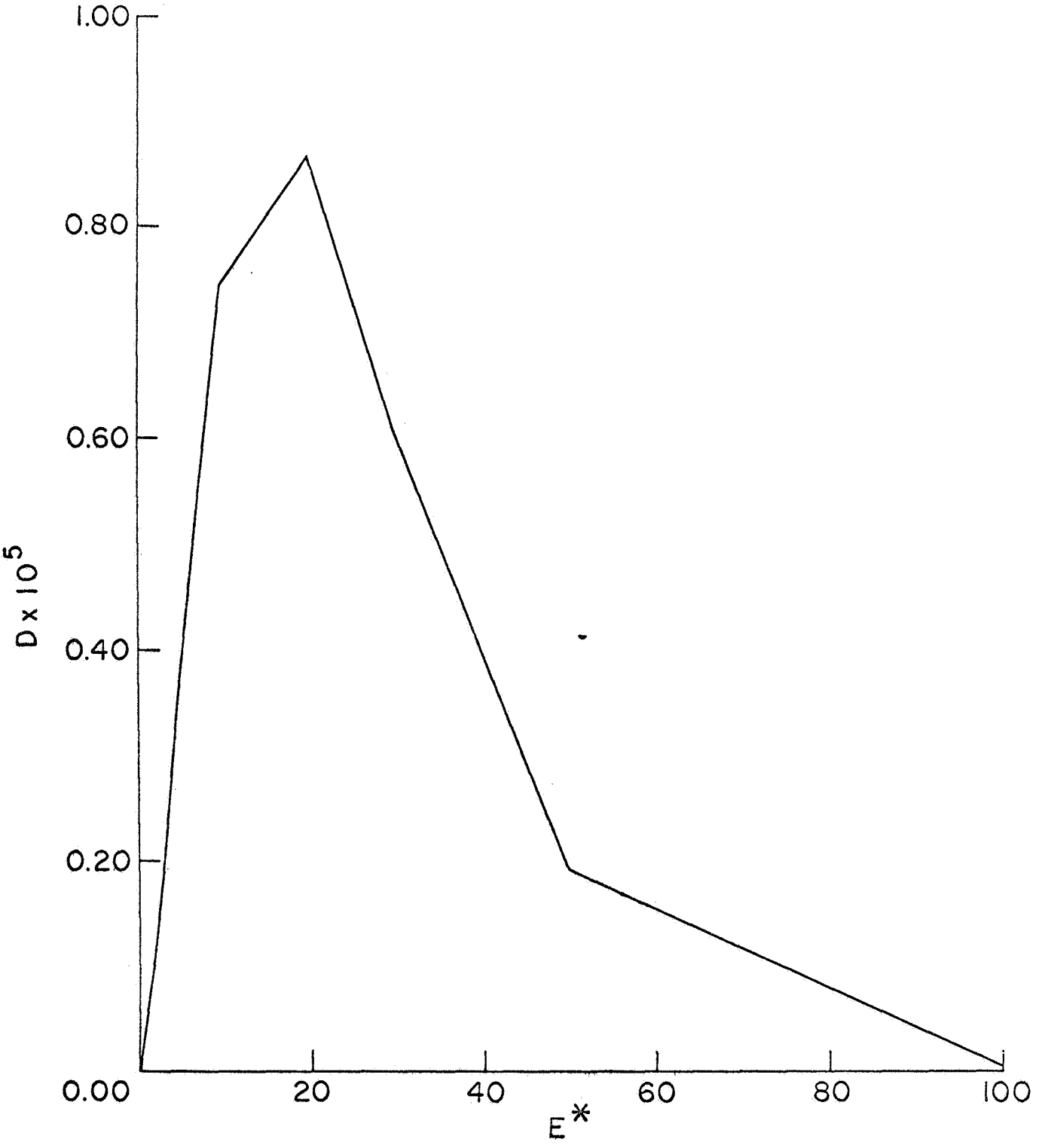

Figure 6a

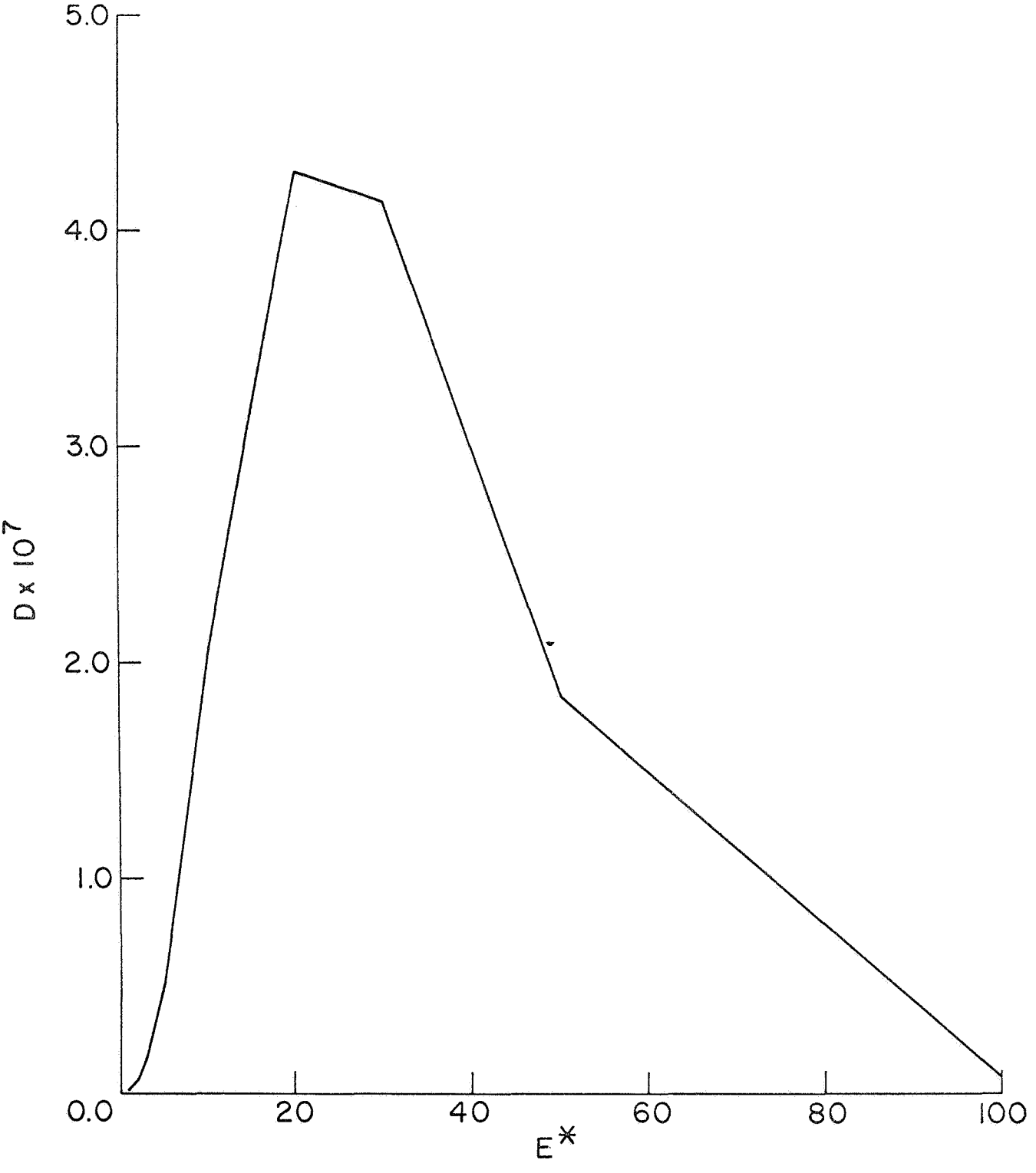

Figure 6b

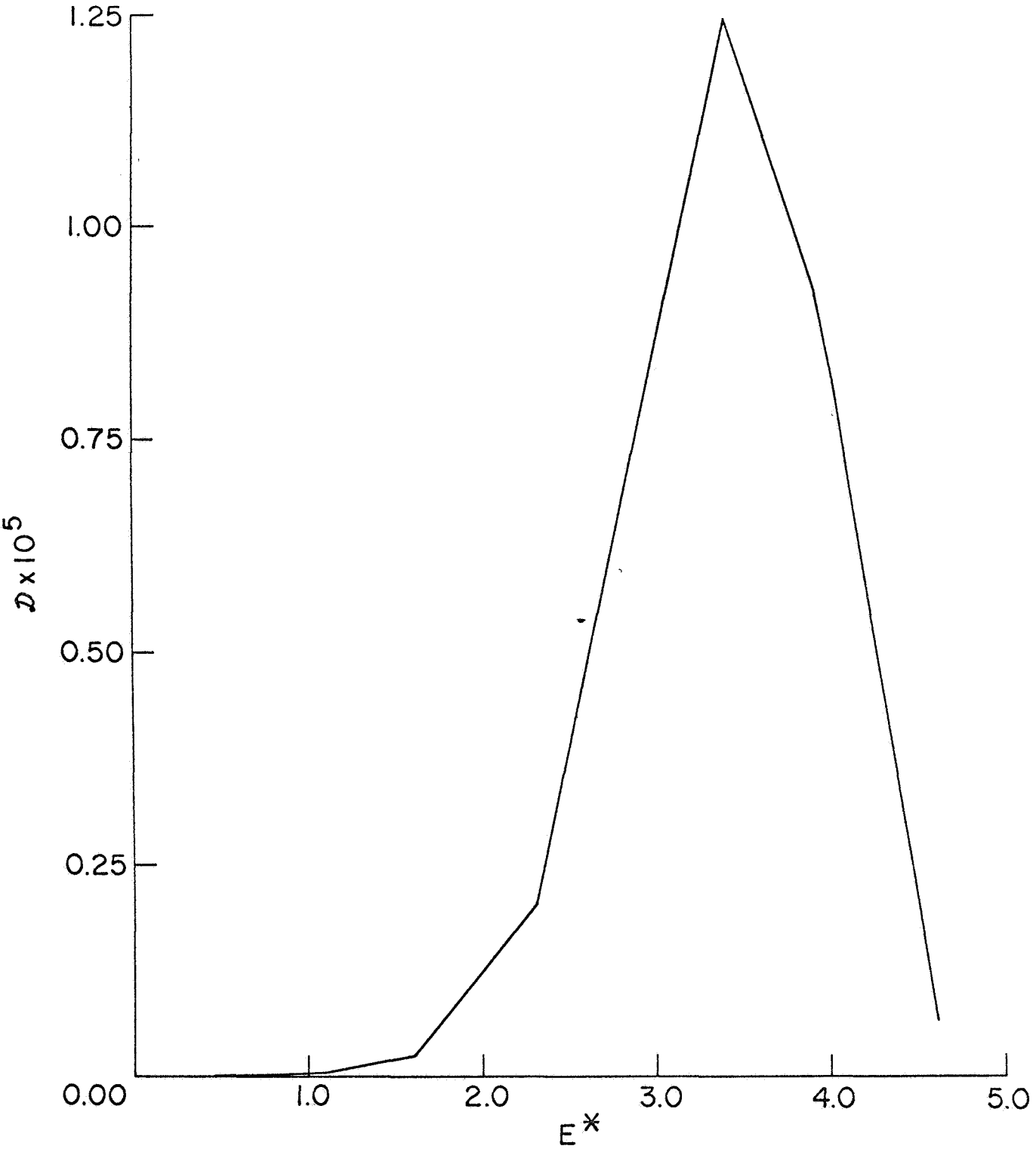

Figure 7a

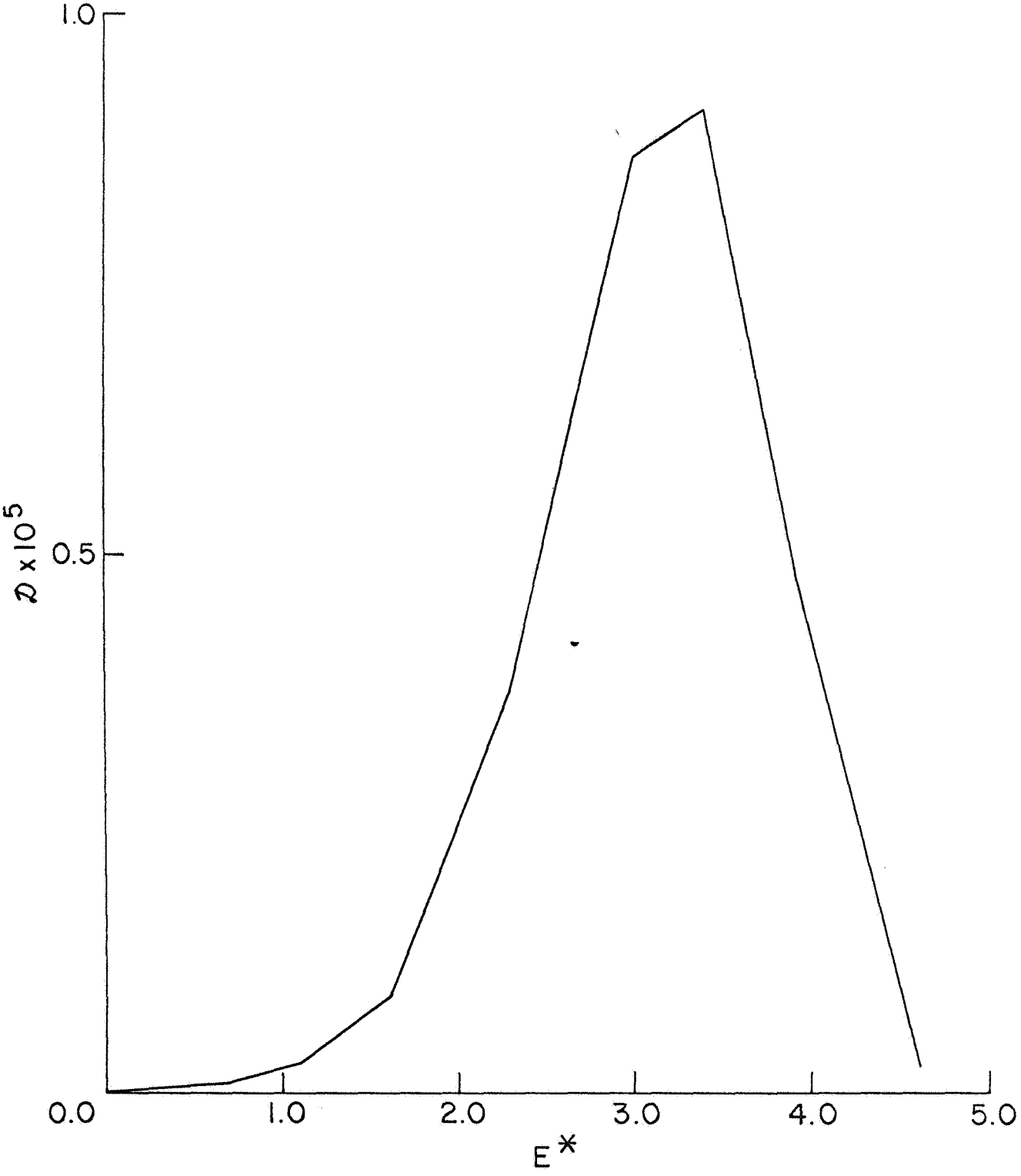

Figure 7b

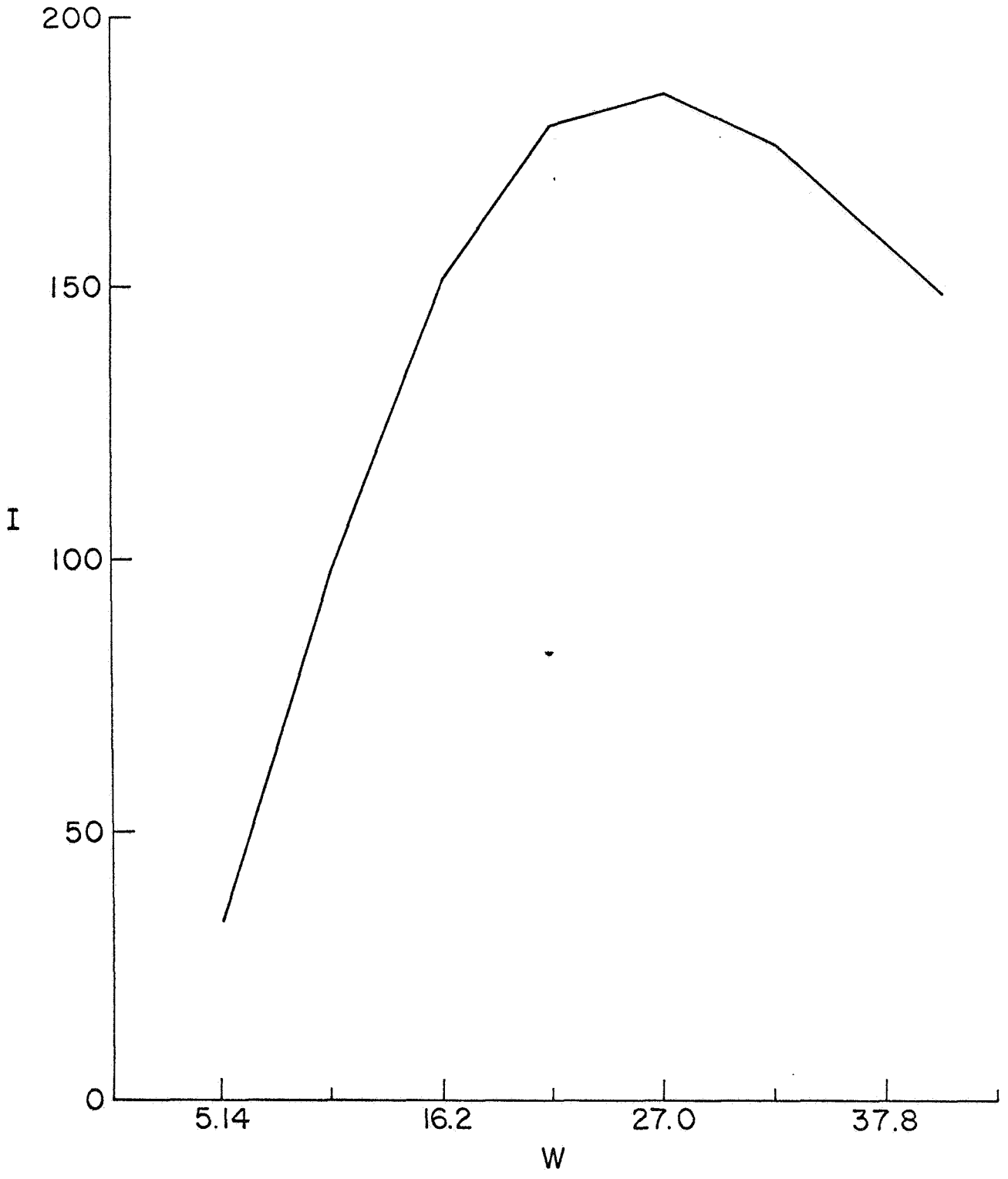

Figure 8

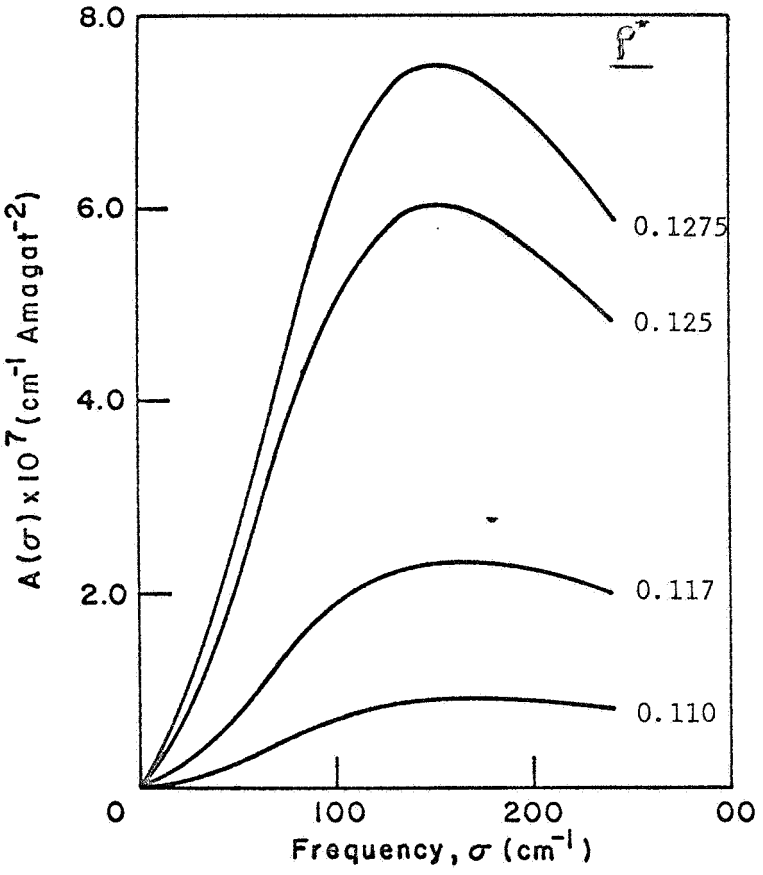
8.0
6.0
4.0
2.0
0
100
200
00
$A(\sigma) \times 10^7 (cm^{-1}\ Amagat^{-2})$
Frequency, σ (cm^{-1})
ρ^*
0.1275
0.125
0.117
0.110

Figure 9

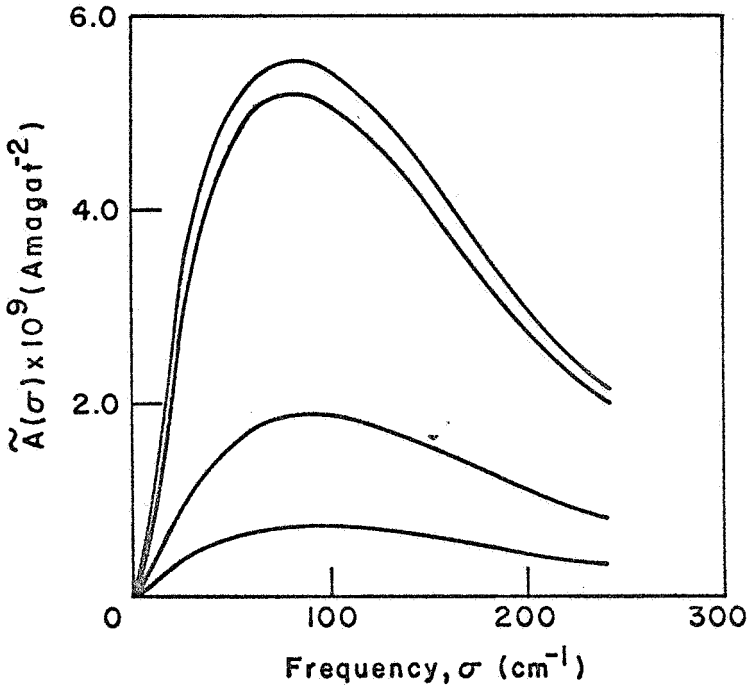
6.0
4.0
2.0
0
100
200
300
$\tilde{A}(\sigma) \times 10^9$ (Amagat^{-2})
Frequency, σ (cm^{-1})

Figure 10

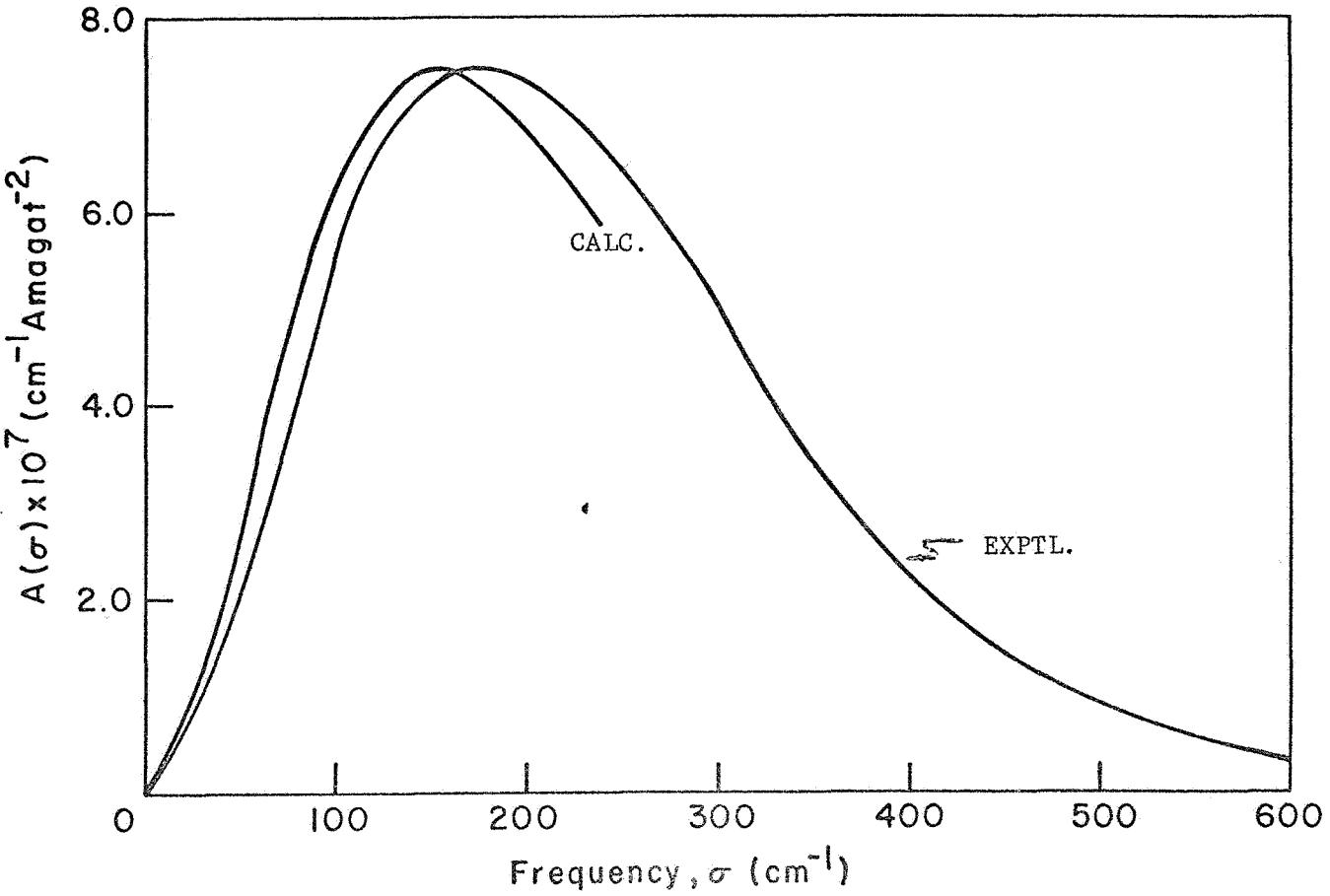
8.0
6.0
4.0
2.0
0
100
200
300
400
500
600
A(σ) x 10^7 (cm^-1 Amagat^-2)
Frequency, σ (cm^-1)
CALC.
EXPTL.

Figure 11

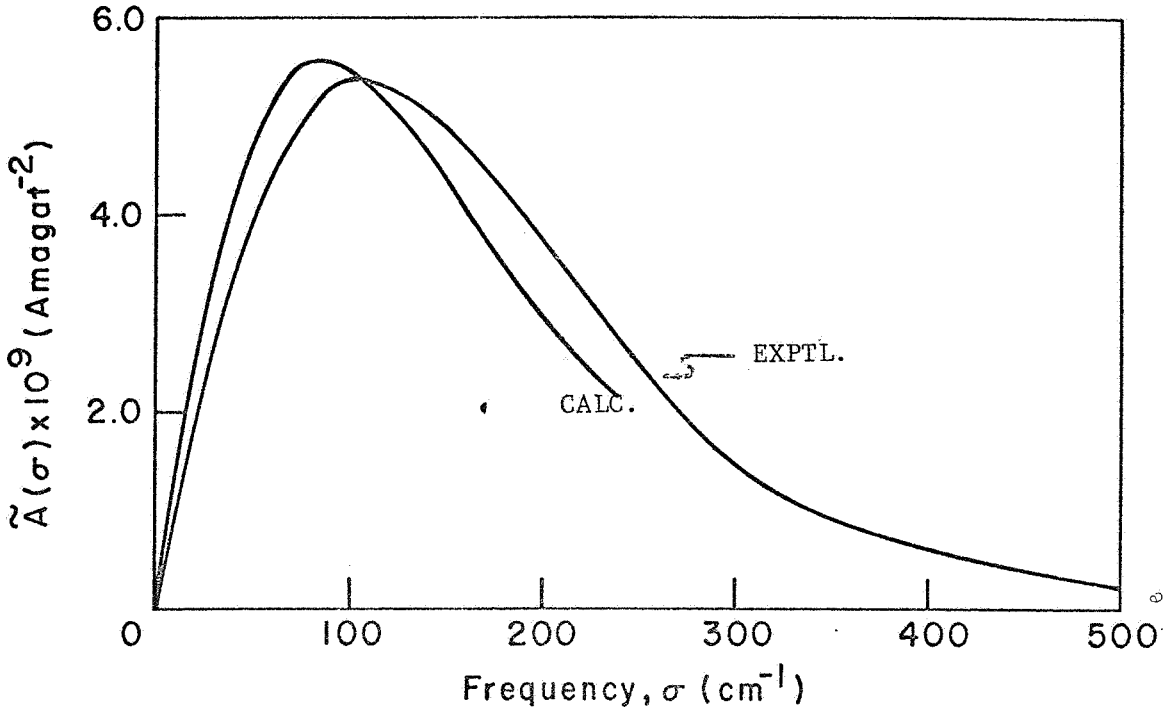
6.0
4.0
2.0
0
100
200
300
400
500
$\tilde{A}(\sigma) \times 10^9$ (Amagat^{-2})
Frequency, σ (cm^{-1})
EXPTL.
CALC.

Figure 12

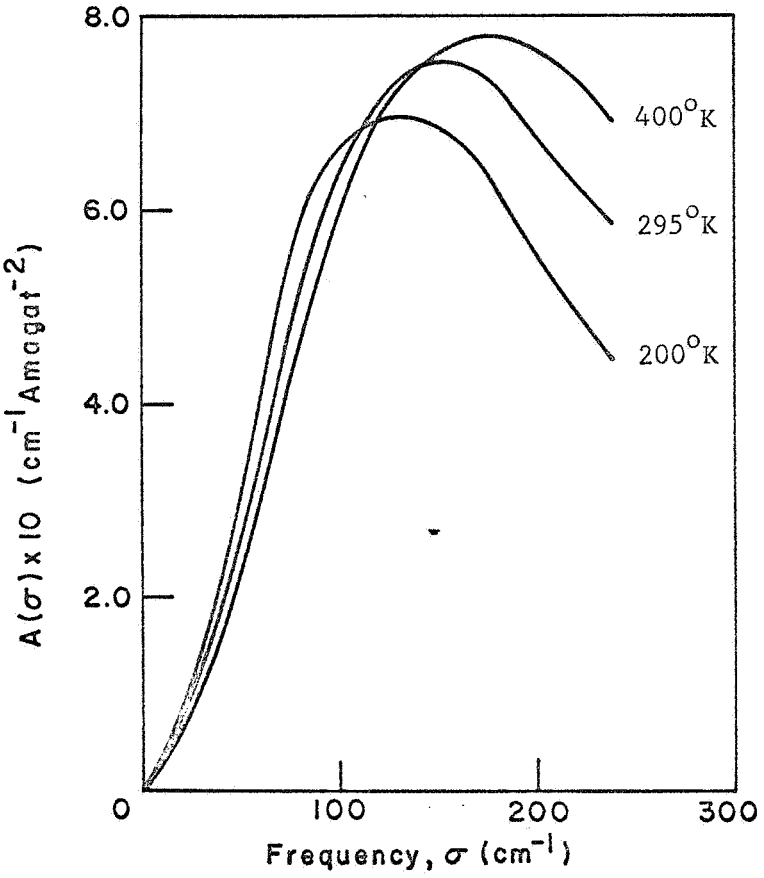
8.0
6.0
4.0
2.0
0
100
200
300
400°K
295°K
200°K
A(σ) x 10 (cm⁻¹Amagat⁻²)
Frequency, σ (cm⁻¹)

Figure 13

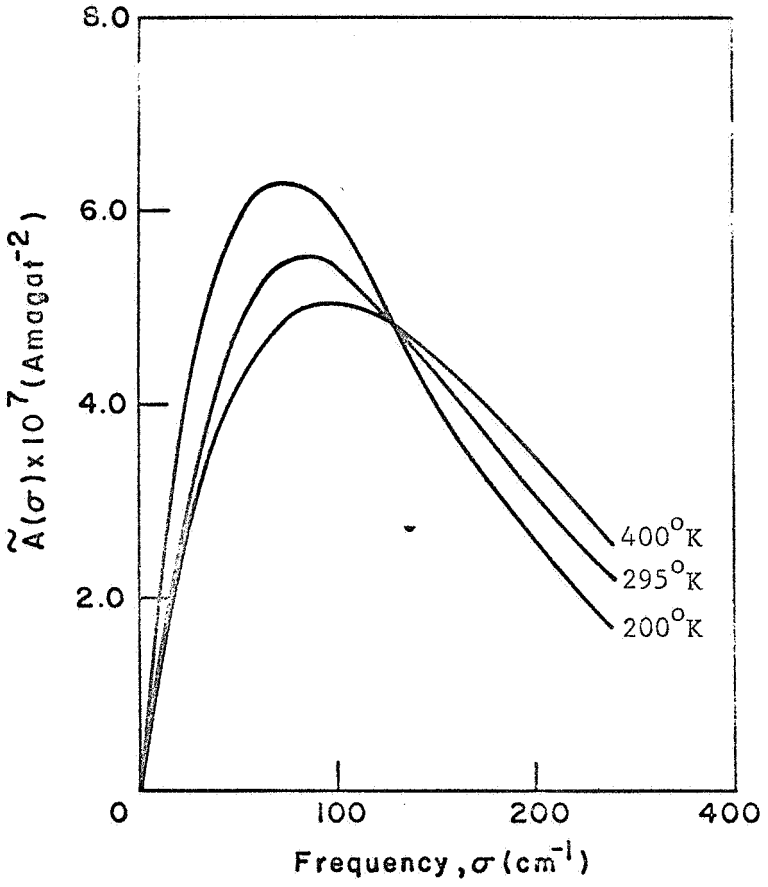
8.0
6.0
4.0
2.0
0
100
200
400
$\tilde{A}(\sigma) \times 10^{7}$ (Amagat^{-2})
Frequency, σ (cm^{-1})
400°K
295°K
200°K

Figure 14

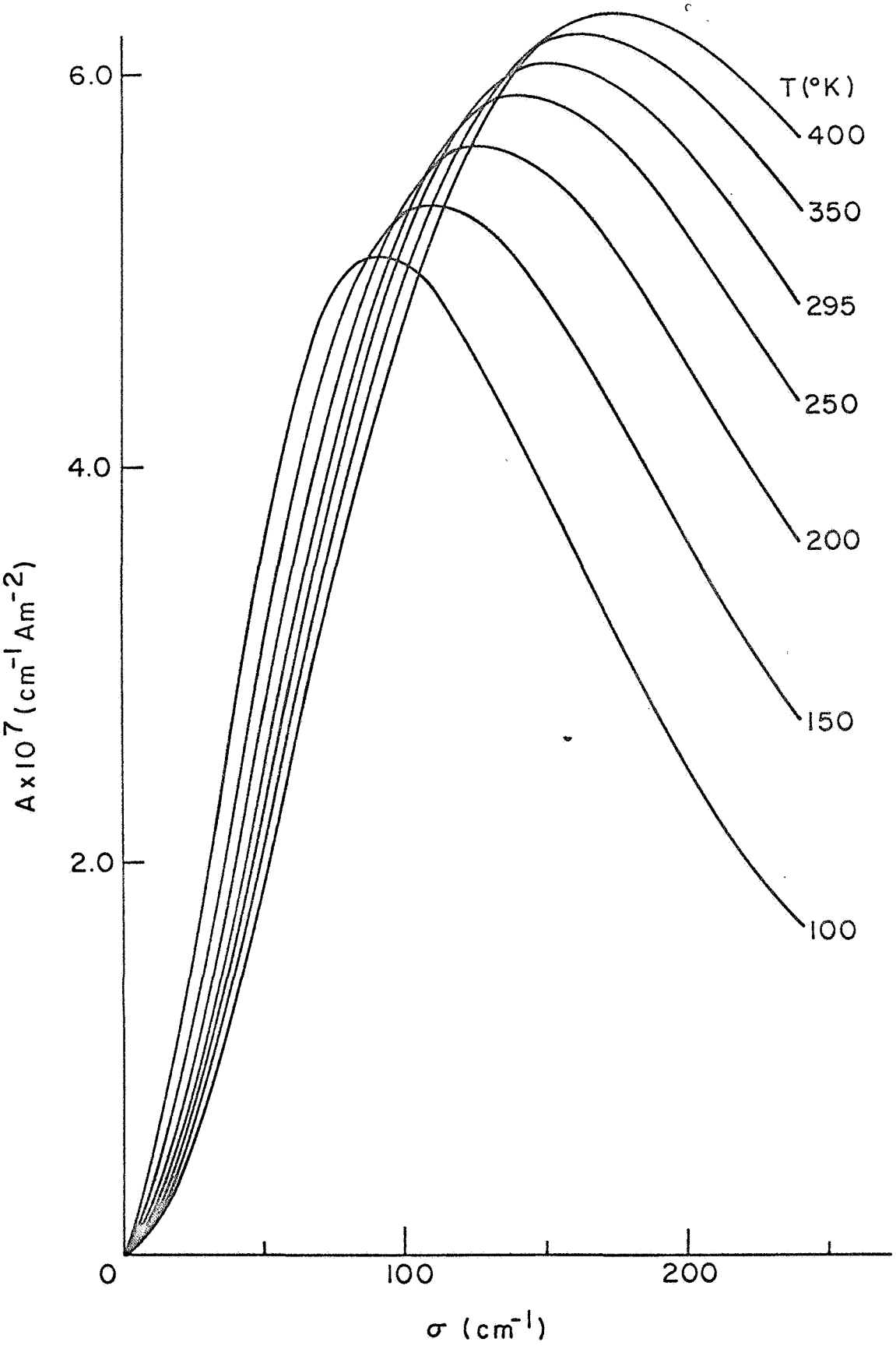
6.0
4.0
2.0
0
100
200
A x 10^7 (cm^-1 Am^-2)
σ (cm^-1)
T(°K)
400
350
295
250
200
150
100

Figure 15